A R C H I V E S O F M E T A L L U R G Y A N D M A T E R I A L S
Volume 53 2008 Issue 2

V.Y. RISONARTA*, L. VOJ*, H. PFEIFER*, H.P. JUNG**, S. LENZ**

OPTIMIZATION OF ELECTRIC ARC FURNACE PROCESS AT DEUTSCHE EDELSTAHLWERKE

OPTYMALIZACJA PROCESU EAF W DEUTSCHE EDELSTAHLWERKE

During stainless steel production in the electric arc furnace (EAF), oxygen is injected to oxidize unwanted tramp elements, mainly carbon and silicon. Unfortunately, oxygen also oxidizes precious elements such as iron and chromium which causes economical loss and bad environmental impact. Off-gas analysis was performed at Deutsche Edelstahlwerke (DEW) to control the decarburization so that the elements, not only carbon, oxidation and oxygen consumption can be controlled as well. This paper presents a new strategy to control the elements oxidation as well as to increase the oxygen efficiency. For the investigated heat, the well controlled decarburization will decrease the oxygen consumption by about 10%. Work was carried out with a financial grant from the Research Fund for Coal and Steel of the European Community.

Keywords: Process control, off-gas analysis, chromium scorification, silicon oxidation, decarburization

Podczas produkcji stali nierdzewnej w elektrycznym piecu łukowym (EAF), tlen jest wdmuchiwany do utlenienia zbędnych domieszek, głównie węgla i krzemu. Niestety tlen również utlenia pożądane składniki jak żelazo i chrom, co powoduje straty ekonomiczne i ma szkodliwy wpływ na środowisko. W Deutsche Edelstahlwerke (DEW) została wykonana analiza gazów wylotowych do sterowania odwęglaniem, również kontrolowane może być utlenianie i zużycie tlenu. W artykule przedstawiono nową strategię kontroli utlenianych składników, w celu zwiększenia wydajności tlenu. Dla badanego nagrzewania, dobrze kontrolowane odwęglanie może zmniejszyć zużycie tlenu o około 10%. Praca została sfinansowana i przeprowadzona w ramach grantu Research Fund for Coal and Steel of the European Community.

1. Introduction

In Germany, 47.2 Mt of steel had been produced in 2006 and 14.7 Mt of them were produced in the EAF [8]. Surging prices of energy and raw materials have encouraged European steel industries for researching new methods in order to reduce the production costs of EAF-steelmaking. Meanwhile, environmental awareness for minimizing the direct and indirect CO_2 emissions among European steel industries has increased during the last few years as well [6]. By minimizing waste and excess material, e.g. through a well-defined process control, European steel industries tend to decrease production cost as well as to give their contribution to decrease the indirect CO_2 emissions from production of raw materials [17]. A new strategy of EAF-route steelmaking is presented here to maintain downward pressure on the above challenges.

During stainless steelmaking at DEW, oxygen is injected mainly to oxidize carbon and silicon. Thus, the amount of oxygen injection is strongly correlated with the initial carbon and silicon input from scrap and alloy elements. Unfortunately, oxygen also oxidizes other elements, e.g. chromium and iron, which are unwanted reactions because it leads to economical loss and bad environmental effects. For this reason, the correlation between the amount of oxygen injection and the amount of carbon and silicon input at DEW had been investigated in this work in order to optimize the amount of oxygen injection as well as to minimize loss of precious elements so that the production cost can be minimized.

Although Ellingham Diagram informs about elements affinity against oxygen, reactions during stainless steelmaking in the EAF are complicated to be well understood since many oxidation and reduction reactions take place in the EAF simultaneously (Table 1). Ellingham Diagram also gives no detail information about interdependency of elements presence on another element oxidation. On the other hand, temperature, oxygen par-

* INSTITUTE FOR INDUSTRIAL FURNACES AND HEAT ENGINEERING, RWTH AACHEN UNIVERSITY, GERMANY
** DEUTSCHE EDELSTAHLWERKE, GERMANY

tial pressure as well as composition of slag and steel melt determine elements oxidation [5, 12]. For this reason, a more detail investigation on interdependency of elements presence on another elements oxidation was carried out. A thermodynamic-based simulation was also performed to investigate more deeply the behaviour of elements oxidation.

TABLE 1
Some oxidation and reduction reactions during stainless steelmaking in the EAF (p = 1 atm, temperature <2200 K)

Reactions	Temperature range for dG < 0 [K]
$2FeO + Si \rightarrow 2Fe + SiO_2 + \Delta H$	Always spontaneous
$FeO + Cr \rightarrow Fe + CrO + \Delta H$	Always spontaneous
$FeO + C \rightarrow Fe + CO + \Delta H$	>997
$FeO + CrO \rightarrow Fe + Cr_2O_3 + \Delta H$	Always spontaneous
$2Cr_2O_3 + 3Si \rightarrow 4Cr + 3SiO_2 + \Delta H$	Always spontaneous
$FeO + CO \rightarrow Fe + CO_2 + \Delta H$	< 832
$Cr_2O_3 + 3C \rightarrow 2Cr + 3CO + \Delta H$	> 1524
$CrO + C \rightarrow Cr + CO + \Delta H$	> 1349
$CrO + CO \rightarrow Cr + CO_2$	Not occurs
$Cr_2O_3 + CO \rightarrow Cr + CO_2$	Not occurs

2. Off-Gas Analysis at the Electric Arc Furnace

In this work, off-gas analysis is utilized to monitor the elements oxidation at DEW. Off-gas analysis was performed at the primary dedusting system. There are two analysis points at EAF, namely point A and point B (Fig. 1). Point A is located directly after the EAF elbow and point B is located about 30 meters far from the EAF elbow to measure off-gas compositions after complete post combustion.

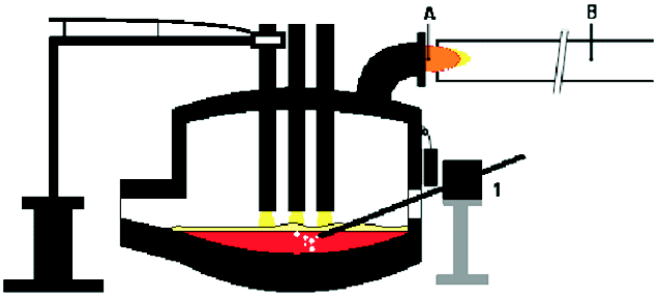

Fig. 1. Point A and point B of off-gas analysis at the EAF dedusting system (1: oxygen lance)

The analyzing equipment consists of water cooled probes, filters, detectors and signal converters for measuring the concentration of off-gas components (CO, CO_2, O_2, H_2), off-gas temperature, and off-gas velocity [10, 11]. The concentrations of the off-gas components were measured by using infrared absorption spectrometry (CO, CO_2), paramagnetism (O_2), and heat conductivity (H_2). The off-gas temperature was measured by coated thermocouples.

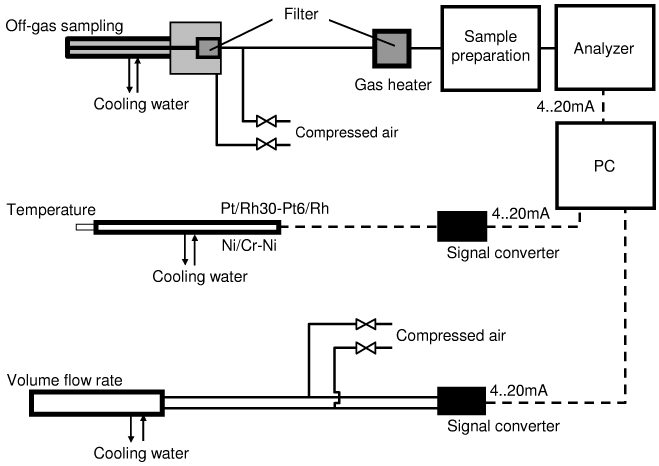

Fig. 2. Sketch of off-gas analysing equipment (off-gas removal and analysing, temperature measurement, volume flow measurement and data acquisition)

The measured data for differential pressure of the gas flow, gas temperature, and off- gas concentrations from the detectors are transformed and recorded continuously. For continuous analysis, probes were installed after complete post combustion in the primary dedusting system [10, 11]. The transportation of the off-gas by pass flow through dust filters and heated tubes to the analyzer causes a time delay of the gas concentration signal. The off-gas volume flow rate and off-gas mass flow rate are calculated from the measured pressure difference of the gas flow, p_{dyn}, and the cross-sectional area of the gas pipe (A) (eq. 1) [10]:

$$\dot{m}_{off-gas} = \rho_{off-gas}\dot{V}_{off-gas} = \\ = \rho_{off-gas}A_{pipe}C\sqrt{\frac{2p_{dyn}}{\rho_{off-gas}}} \quad (1)$$

ρ(T) is the gas density depending on gas temperature and off-gas composition. Measured off-gas mass flow rates at points A and B were checked with carbon mass flow rates and complete carbon mass balances. The time-dependent value was integrated over the heat time to obtain mean values.

3. Simulation of Elements Oxidation

A simulation was performed to investigate the elements oxidation during oxygen injection (Fig. 3). The simulation is only based on thermodynamic equilibrium

and does not take account on any other influencing processes, e.g. heat and mass transfer and kinetics. Uniform elements and temperature distribution were assumed in this simulation.

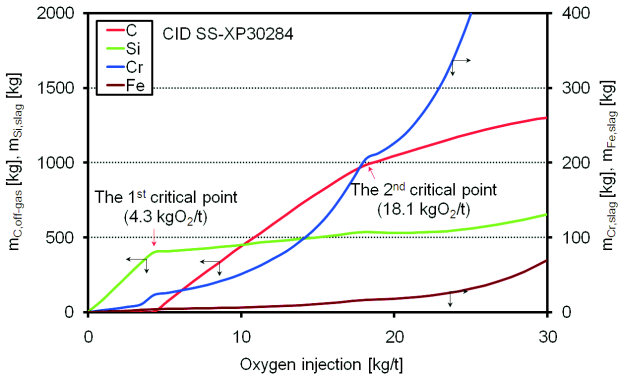

Fig. 3. A thermodynamic-based simulation of elements oxidation

Simulation result shows an intensive silicon oxidation in the early stage of oxygen injection and this is in agreement with result of other researchers [7, 20]. Ellingham Diagram informs that silicon is relatively easily oxidized compared to other elements due to lower Gibbs free energy of its oxidation. In this particular heat, the intensive silicon oxidation is finished at 4.3 kgO_2/t and then silicon-lean condition in melt occurs. Due to the decreasing silicon concentration in melt (x_{Si}), the silicon activity in the melt (a_{Si}) decreases because the activity coefficient of silicon (γ_{Si}) is constant at this low concentration following Henry's law (eq. 3).

$$a_{Si} = \gamma_{Si} x_{Si} \tag{2}$$

Under this circumstance, carbon and chromium starts to oxidize intensively. The increase of carbon activity with decreasing silicon content in the melt is in agreement with the result of other researchers [1, 12, 18]. Then, finishing the intensive silicon oxidation below 4.3 kgO_2/t, e.g. by changing the composition of elements input so that the silicon activity can be influenced, could lead to earlier intensive carbon oxidation.

Chromium oxidizes intensively after the intensive silicon oxidation is finished. Meanwhile, iron is oxidized in small amount in the beginning and starts to oxidize exponentially after carbon oxidation reach the 2nd critical point at about 18.1 kgO_2/t.

4. Monitoring of Elements Oxidation during Oxygen Injection

Results of off-gas analysis and slag analysis are utilized here to investigate the occurrence of intensive oxidation for some elements during stainless steelmaking in the EAF. A decarburization model based on off-gas analysis is then presented (Fig. 4). This decarburization model can be utilized to monitor not only carbon oxidation but oxidation of other elements as well. The decarburization model shows three stages of oxygen injection, i.e. early stage, middle stage and end stage. The 1st critical point of oxygen injection ends the early stage. The middle stage lies between the 1st and the 2nd critical points and the end stage starts after the 2nd critical point of oxygen injection is reached.

Differences between simulation result and the result of off-gas analysis was identified since the simulation is based only on a thermodynamic equilibrium conditions. As an example, the thermodynamic-based simulation result shows no occurrence of carbon oxidation until the 1st critical point is reached. Meanwhile, the decarburization model shows that carbon oxidation, although not intensive, occurs since the early stage of oxygen injection. The differences exist because the elements oxidation and reduction does not depend merely on thermodynamic condition but on many other processes, e.g. mass and heat transfer, fluid mechanics, and kinetics, as well (1). The differences come also from non-uniformity of temperature and elements, including oxygen, distribution (2). The injection zone lying directly after the oxygen lance has the highest oxygen content as well as has the highest temperature which leads to higher carbon oxidation [2, 13]. At DEW, the size of the injection zone depends on the lance position, oxygen mass flow rate, as well as steel scrap density and composition [13].

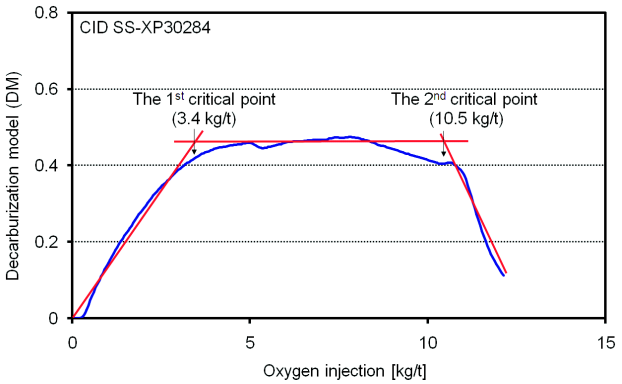

Fig. 4. Decarburization model

Nevertheless, a similarity between the simulation result and off-gas analysis exists. Similar to the simulation result, the decarburization model shows that intensive carbon oxidation occurs after intensive silicon oxidation is finished. The decarburization model shows two critical points as well, i.e. the 1st and the 2nd critical points. In this particular heat, carbon starts to oxidize intensively after oxygen injection reaches the 1st critical point at 3.4 kgO_2/t. The 1st critical point in the decarburization model at 3.4 kgO_2/t refers to the end of intensive silicon

oxidation at 4.3 kgO2/t in the simulation result (Fig. 3). Meanwhile, the 2nd critical point at 10.5 kgO_2/t in the decarburization model refers to the starting point of declining decarburization at 18.1 kgO_2/t in the simulation result.

In agreement with the simulation result, analysis of slag and tapped steel show that silicon is oxidized intensively in the early stage of oxygen injection. Due to low silicon content in the tapped steel, silicon-containing reduction agent, e.g. ferrosilicon is added to increase the silicon content in the melt as well as to recover the precious elements from oxides. Liquid phase mass transfer controls the desiliconization rate $\left(\frac{d\%\mathrm{wt}_{Si}}{dt}\right)$ in the early stage of oxygen injection (eq. 4) [7]. In this stage, the desiliconization rate depends on the surface area of reaction site (A), steel density (ρ_{St}), steel weight (W_{St}), overall coefficient of silicon mass transfer (k_{Si}), current silicon content in the melt ($\%\mathrm{wt}_{Si}$), and the equilibrium silicon content in the melt ($\%\mathrm{wt}_{Si,eq}$) [5, 7].

$$\frac{\mathrm{d}\%\mathrm{wt}_{Si}}{\mathrm{dt}} = -\frac{A\rho_{st}k_{Si}}{W_{st}}\left(\%\mathrm{wt}_{Si} - \%\mathrm{wt}_{Si,eq}\right) \qquad (3)$$

Consequently, enhancing conditions, e.g. good mixing and high contact area between silicon and oxygen, are necessary to improve desiliconization rate in this stage.

Both simulation result and decarburization model show that carbon oxidizes intensively in the middle stage. The decarburization rate in this stage depends linearly on the flow rate of oxygen injection since the decarburization in this stage is controlled by chemical reaction [5, 13]. Because the decarburization in this stage depends on the mass flow rate of oxygen injection, the decarburization model can be utilized to monitor the effectiveness of the oxygen injection process, e.g. optimization of lance depth, bubbling condition, attack angle, oxygen velocity, lance diameter, etc. These factors are influencing the injection zone and oxygen distribution in the melt.

After the oxygen injection reaches the 2nd critical point, decarburization rate declines with further oxygen injection because carbon activity (a_C) in the melt is already low due to decreasing carbon content in the melt below its critical level following Henry's law (1). Besides due to decreasing carbon activity, declining decarburization rate in this end stage occurs due to decreasing driving force of decarburization kinetic with decreasing carbon content in the melt as well (2) [9, 13]. In this end stage, mass transfer of carbon controls the decarburization [13, 20] and the decarburization rate $\frac{d\%\mathrm{wt}_C}{dt}$ depends on the current carbon content in steel ($\%\ \mathrm{wt}_C$), the equilibrium carbon content ($\%\mathrm{wt}_{C,eq.}$), mass transfer coefficient for the particular reaction site (k_i) as well as area of the specific reaction site (A_i) (eq. 5) [7].

$$\frac{d\%\mathrm{wt}_C}{dt} = -\frac{\rho_{st}}{W_{st}}\left(\%\mathrm{wt}_C - \%\mathrm{wt}_{C,eq}\right)\sum_{i=1}^{j} k_i A_i \qquad (4)$$

In this carbon-lean condition, oxygen prefers to oxidize precious elements, e.g. chromium and iron, instead of carbon. A good mixing condition to enhance the decarburization in the end stage can be developed by injecting stirring gas, e.g. nitrogen or argon.

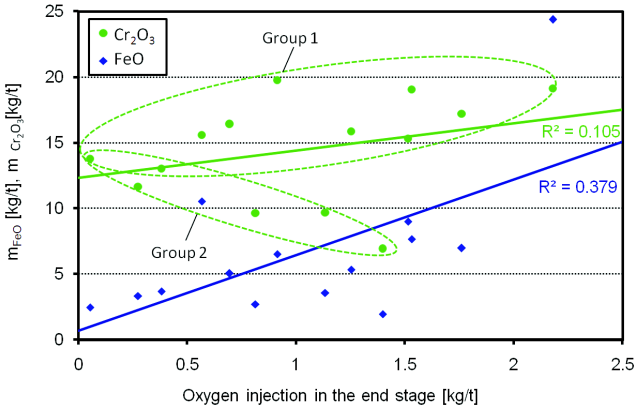

Fig. 5. Influence of further oxygen injection in the end stage on chromium and ferrous oxidation (before application of the decarburization model)

An opportunity to save the oxygen consumption by about 10%, or equal to 1.5 kgO_2/t, exists for the investigated heat since the oxygen injection can be finished directly after the 2nd critical point is reached. Besides saving the oxygen consumption, finishing the oxygen injection at the 2nd critical point will minimize iron oxidation as well because intensive FeO formation occurs in the end stage of oxygen injection (Fig. 5). High iron oxidation in the end stage occurs due to increasing iron activity in the melt with decreasing carbon and silicon content in the melt (Fig. 6). Silicon content in the melt decreases due to its intensive oxidation in the early stage and the carbon in the steel melt is already oxidized intensively before the 2nd critical point is reached. The non-zero coefficient of regression line at 0.7 kg_{FeO}/t (Fig. 5) shows that iron oxidation already takes place, although not so intensive, in the early and middle stage. Due to its higher non-zero coefficient at 12.3 kg_{Cr2O3}/t, it is shown that chromium is oxidized more intensively than iron before the end stage is reached. This is in agreement with the simulation result in Fig. 3.

Chromium oxidation shows a slightly different behaviour compared to iron oxidation. iron oxidation shows a definite correlation between FeO formation and further oxygen injection after the 2nd critical point is reached. In the other hand, there are two different groups of Cr_2O_3 formation results (Fig. 5). The first group has a positive correlation between chromium oxidation and the amount

of oxygen injection in the end stage and the second group has a negative correlation, vice versa. This is suggesting a weak correlation between the amount of oxygen injection in the end stage and Cr_2O_3 content in the slag.

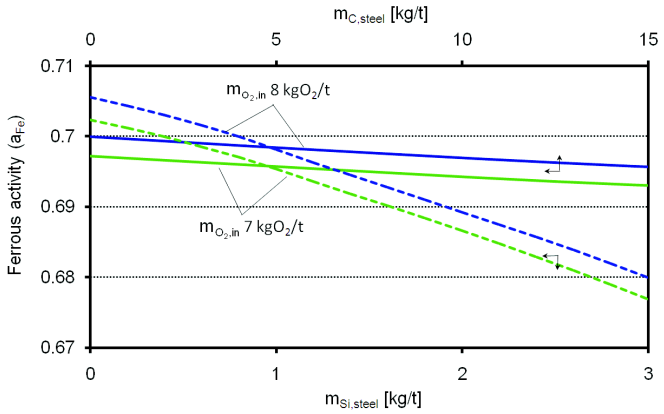

Fig. 6. Influence of carbon and silicon content in steel on iron activity (simulated)

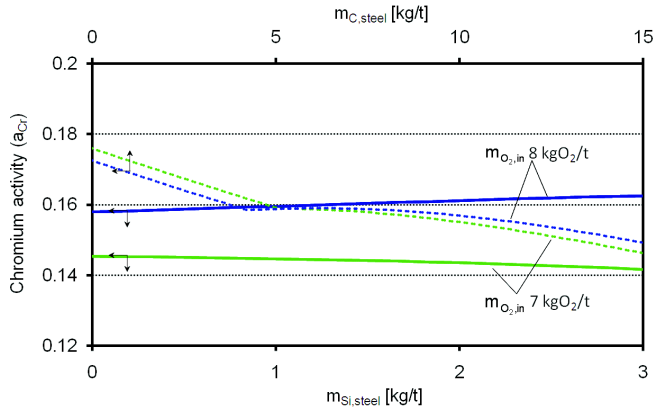

Fig. 7. Influence of carbon and silicon content in steel on chromium activity (simulated)

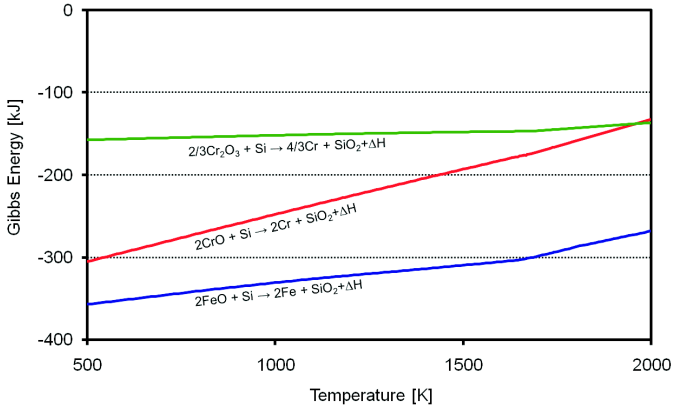

Fig. 8. Gibbs free energy of FeO and Cr_xO_yreduction by silicon

Simulation result also shows these two different groups (Fig. 7). The simulation shows a negative correlation between carbon content in melt and chromium activity. Voj [19] also reported a negative correlation between carbon content in steel and chromium oxidation. However, decreasing chromium activity with increasing carbon content in melt is not as clear as the correlation between carbon content and iron activity in Fig. 6. Ma and Janke [12] reported that the chromium activity in the melt (a_{Cr}) does not correlate linearly with the chromium content in the melt (x_{Cr}). Above the optimum value, chromium content in the melts correlates negatively with the chromium activity. Irregularity is also shown here since the chromium activity for oxygen input at 8 kgO_2/t is higher than for oxygen input at 7 kgO_2/t when the carbon content in melt exceeds 5.1 kg/t. Unlike the influence of silicon content on iron activity (Fig. 6), the influence of silica content on chromium activity in Fig. 7 shows an inverse correlation which depends on the amount of oxygen input.

Besides preventing further direct chromium oxidation by oxygen (1), finishing the oxygen injection at the 2nd critical point will minimize chromium oxidation by FeO after tapping (2) (Table 1) and improve efficiency of the Cr_xO_y reduction, e.g. by Si, as well (3) (Fig. 8). Minimum iron oxidation leads to more effective Cr_xO_y reduction since Cr_xO_y reduction does not compete with FeO reduction. FeO reduction is thermodynamically more preferable than Cr_xO_y reduction since Gibbs free energy of FeO reduction is comparably lower than that of Cr_xO_y reduction. At temperature 2000 K, Gibbs free energy of FeO reduction by silicon is about two times lower than that of Cr_xO_y reduction. Gibbs free energy of FeO reduction at temperature 2000 K is −267 kJ, while Gibbs free energy for CrO and Cr_2O_3 reduction by silicon are −133 kJ and −132 kJ, respectively. At temperature higher than 1960 K, silicon prefers to reduce Cr_2O_3 than CrO.

5. Important Factors for Silicon Oxidation

Influencing factors for intensive silicon oxidation during oxygen injection was investigated because the end of intensive silicon oxidation is correlated with the beginning of intensive decarburization. If intensive silicon oxidation could be finished earlier, the intensive decarburization could be started earlier as well. In case intensive carbon oxidation could be started earlier, i.e. the 1st critical point is shifted to the left side; too deep desiliconization could be prevented (1) and the oxygen consumption could be reduced as well because the 2nd critical point could be shifted to the left (Fig. 4) (2).

As informed previously, silicon and carbon oxidation have influence on presence of other elements. Here, decarburization reaction takes place earlier from 6.6 kgO_2/t down to 5.4 kgO_2/t as the ratio between carbon input and silicon input increases by 50% (Fig. 9).

Vice versa, carbon oxidation starts earlier if the ratio between iron input and silicon input decreases (Fig. 10).

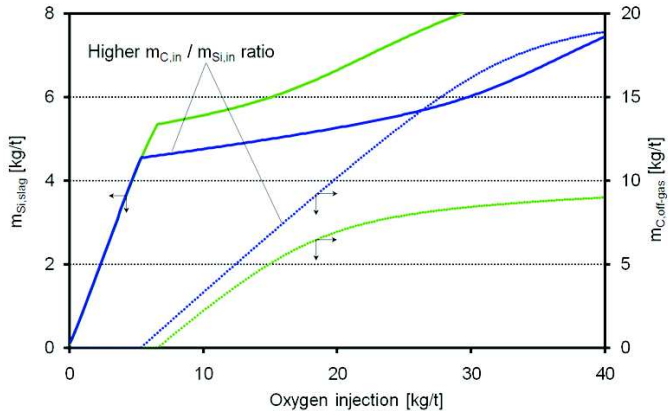

Fig. 9. Influence of higher carbon-silicon ratio on silicon oxidation (simulated)

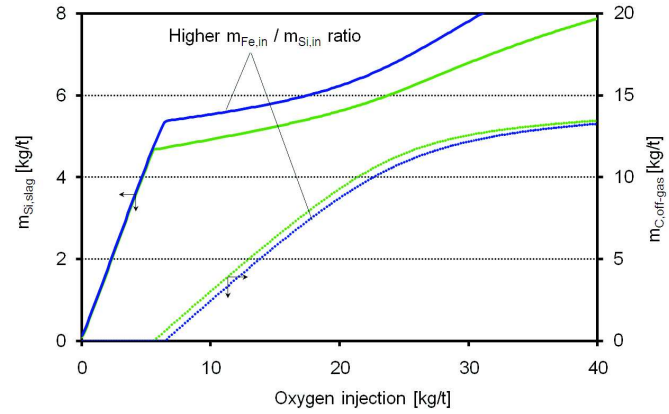

Fig. 10. Influence of higher iron-silicon ratio on silicon oxidation (simulated)

6. Application of the Decarburization Model

Since the concept of decarburization model is based on off-gas analysis, a dynamic real-time process control is possible to be developed. This decarburization model can be visualized into the computer screen, so that the EAF operator can finish the oxygen injection if the decarburization model shows the declining tendency after the 2nd critical point is reached. Besides the application in the EAF, monitoring of elements oxidation, not only decarburization process, through the off-gas analysis could be performed for other decarburization-related process, e.g. converter.

Application of the decarburization model can directly decrease the iron and chromium oxidation what is beneficial for many production parameters. Yield of mass of tapped steel increases as higher iron and chromium oxidation can be prevented. As a consequence, mass of unwanted elements, e.g. carbon and silicon [%wt], can be decreased by increasing iron and chromium mass in the tapped steel [kg]. The specific value of production parameters, e.g. O_2 consumption [kg/t] and productivity [t/h], change as well. Besides contribution from higher tapping mass [t], lower specific oxygen consumption [kg/t] was obtained also from decreasing actual oxygen consumption [kg]. Consumption of added reduction agent, e.g. FeSi, decreases since the content of ferrous and chromium oxide in the slag can be minimized.

7. Summary

Maximum decarburization and minimum oxidation of chromium and iron are beneficial for stainless steelmaking in the EAF. In this work, optimization of elements oxidation at Deutsche Edelstahlwerke (DEW) was performed through off-gas analysis. Decarburization is closely correlated not only with the amount of oxygen injection but with presence of other elements as well. Since the oxygen demand for silicon and carbon oxidation does not depend merely on silicon and carbon input, a new correlation to calculate the oxygen demand has been presented. Results from a thermodynamic-based simulation combined with slag and off-gas analysis showed a good opportunity to monitor elements oxidation through off-gas analysis. A new EAF process control based on off-gas analysis had been presented. By finishing the oxygen injection at the 2nd critical point in the decarburization model, high iron and chromium oxidation can be prevented. For the investigated heat, application of the decarburization model will reduce the oxygen consumption by about 10%.

Acknowledgements

Financial support from the European Community Research Fund for Coal and Steel, Contract no. RFSR-CT-2006-00004, is acknowledged.

REFERENCES

[1] N. Anacleto, O. Ostrovski, S. Ganguly, Carbon solubility and phase composition of silicomanganese, steel research **77**, 4, 227-233 (2006).

[2] S. Arnout, F. Verhaeghe, B. Blanpain, P. Wollants, R. Hendickx, G. Heylen, A thermodynamic model of the EAF process for stainless steel, steel research, **77**, 5, 317-323 (2006).

[3] M. Barati, K.-S. Coley, A comprehensive kinetic model for the CO-CO_2reaction with iron oxide-containing slags, metallurgical and materials transactions B, **37B**, 61-69 (2006).

[4] J.-G. B e k k e r, Modelling and control of an electric arc furnace off-gas process, Master thesis, University of Pretoria, Faculty of Mechanical Engineering, 1998.

[5] B. D e o, R. B o o m, Fundamentals of steelmaking metallurgy, Prentice Hall International, 1993.

[6] Eurofer: The greenhouse gas challenge: How the EU steel industry competitiveness could be affected, position paper, January 2005.

[7] R.-F. F r u e h a n, The making, shaping and treating of steel: steelmaking and refining volume, 11^{th}edition, The AISE Steel Foundation, Pittsburgh, 1998.

[8] International iron and steel institute (IISI): World steel in figures 2007, September 2007.

[9] Y. K a t o, H. O k u d a, Reaction model for carbon, manganese and oxygen in bottom blowing with mixed gas in final stage of steel refining in converter, ISIJ international, **43**, 11, 1710-1714 (2003).

[10] M. K i r s c h e n, R. K ü h n, S. L e n z, J. L o h, H. P f e i f e r, K. S c h a e f e r s, F. W a h l e r s, Off-gas measurements at primary dedusting system of electric arc furnace, stahl und eisen, **124**, 11, 73-89 (2004).

[11] M. K i r s c h e n, H. P f e i f e r, F. W a h l e r s, H. M e e s, Off-gas measurements for mass and energy balances of stainless steel EAF, Proc. of 59th Electric Furnace Conference, Arizona, USA, Nov. 11-14 2001, 737-745.

[12] Z. M a, D. J a n k e, Thermodynamic assessment to chromium oxidation in the production of stainless steel, steel research, **74**, 2, 99-103 (2003).

[13] F. O e t e r s, Metallurgy of steelmaking, Verlag Stahleisen mbH, Düsseldorf, 1994.

[14] H. O n o-N a k a z a t o, Y. M o r i t a, K. T a m u r a, T. U s u i, K. M a r u k a w a, Oxidation behaviour of silicon and carbon in molten iron-carbon-silicon alloys with carbon dioxide, ISIJ international, **41** Supplement, S61-S65 (2001).

[15] H. P f e i f e r, M. K i r s c h e n, Thermodynamic analysis of EAF energy efficiency and comparison with a statistical model of electric energy demand, Proc. of 7th European Electric Steelmaking Conference, Venice, Italy, May 26-29, 1413-1428 (2002).

[16] L.-P. R a t h a b a, Model fitting for electric arc furnace refining. Master thesis. University of Pretoria, Faculty of Mechanical Engineering, 2004.

[17] V. R i s o n a r t a, L. V o j, M. K i r s c h e n, C. B e i l e r, B. E l e z i, H. P f e i f e r, Reduction of CO_2 emissions and optimization of EAF energy input, Proc. of 35th McMaster University Iron and Steelmaking Symposium, Hamilton, Canada, June 5-7 2007.

[18] K. T a n g, V. O l s o, O. S v e r r e, Manganese and silicon activities in liquid carbon-saturated Mn-Si-alloys, steel research, **73**, 3, 77-81 (2002).

[19] L. V o j, Installation of a permanent off-gas measurement for process control of a 140-t EAF, Diploma thesis, Institute for Industrial Furnaces and Heat Engineering in Metallurgy, RWTH Aachen University, August 2002.

[20] F.-J. W a h l e r s, K.-H. S c h u b e r t, C. B u r k a t, S. K ö h l e, C. B e n d e l, Observation and control of AOD process with exhaust gas measurement, Proc. of Electric Furnace Conference, Orlando, 893-903 USA, 2000.

Received: 3 April 2008.